Optica Applicata, Vol. LV, No. 2, 2025
DOI: 10.37190/oa/200435

Plasmonic wave at uniaxial chiral-metal-uniaxial chiral interface

M. Umair[1,*], A. Ghaffar[1,*], Majeed A.S. Alkanhal[2], Y. Khan[2], M. Amir Ali[3]

[1]Department of Physics, University of Agriculture, Faisalabad, Pakistan

[2]Department of Electrical Engineering, King Saud University, Riyadh, Saudi Arabia

[3]School of Materials Science and Engineering, Zhengzhou University, Zhengzhou 450001, China

[*]Corresponding authors: majeed@ksu.edu.sa (MU), aghaffar16@uaf.edu.pk (AG)

This work examines the propagation of light plasmon coupling at uniaxial chiral-metal-uniaxial chiral planar interface. Gold (Au) is sandwiched between uniaxial chiral (UAC) layers. We have derived the characteristics equation by employing boundary conditions at $x = d$ on UAC-metal and $x = -d$ on metal-UAC interfaces. Three cases of UAC medium are discussed under the different values of chirality and core width in the visible frequency region. Based on the numerical results, it is concluded that case I ($\varepsilon_t = -0.025\varepsilon_0$, $\varepsilon_z = 0.2\varepsilon_0$) has the highest effective mode index (EMI), whereas case II ($\varepsilon_t = 0.25\varepsilon_0$, $\varepsilon_z = -0.2\varepsilon_0$) has the lowest EMI. As an additional benefit, it has also been shown that a specified frequency band can be tuned by altering the chirality and core width of the proposed planar structure. Moreover, case III ($\varepsilon_t = -0.25\varepsilon_0$, $\varepsilon_z = -0.5\varepsilon_0$) exhibits the highest cut-off frequency and case I exhibits the lowest value. The present work may have potential applications in optical sensors, plasmonic platforms, detectors and surface waveguides.

Keywords: plasmonics, uniaxial chiral, effective mode.

1. Introduction

The application of electromagnetic surface waves in the field of plasmonics has recently garnered significant attention from researchers due to their potential applications in various areas, including communications, optoelectronic devices, light-trapping systems, spectroscopy, and biochemical sensing. Different types of EM surface waves, like the surface plasmon polaritons (SPPs) [1-3], Fano, Tamm, Dyakonov, and Bloch waves, propagate through specific interfaces [4]. In the past few decades, SPPs have been extensively researched for their multiple unique properties, which have been leveraged to design nanoscale electronic and photonic devices [1-5]. SPPs are the phenomenon by which electromagnetic waves propagate along a metal surface, unlike within a dielectric waveguide. The SPPs can be used for controlling switches and constructing amplifiers and modulators [6-10]. An essential difference between SPPs and conventional focusing technologies such as dielectric lenses is that

SPPs are capable of confining electromagnetic fields to smaller scales, which makes them distinct from conventional focusing techniques [1, 11]. By substituting SPPs for free-space propagating EM waves, it is possible to reduce the size of devices and systems. Interaction between photons and electrons produces a larger wavevector than free space waves [12]. Thus, it is evident that metal-based structure plays a key role in determining the frequency range as well as propagation loss of SPPs modes [13]. Several metal-based structures have been developed for the excitation of SPPs [5-7, 14-16]. Using SPPs, optical signals can be transmitted beyond the diffraction limit. Metals exhibit novel optical properties due to their quasi-free electrons. Electrons exhibit optical properties as they oscillate in an electric field. Metals can confine photons in the visible spectrum at subwavelength scales [8]. Additionally, when the energy of the photon exceeds the energy of the metal's bandgap, there is a possibility of interband excitations. Freely moving conduction electrons can have a significant effect on noble metals properties [9]. Various metal-based studies were presented to explore SPPs characteristics. Mi *et al*. examined the plasmonic properties of SPPs at chiral metal interfaces [15]. A theoretical model of the characteristics of EM surface waves at chiral metal-chiral planar interfaces has been developed by Zhang *et al*. to design nanophotonic devices [10]. Scientifically, waveguides based on chiral SPPs are also subject to increasing attention in the scientific community. Furthermore, it has been demonstrated that the presence of localized chiral SPPs in symmetric nanostructure enables chiral sensing of small chiral molecules, while propagating chiral SPPs in one-dimensional metal nanowires enables high-resolution microscopy and spectroscopy. However, one of the major disadvantages of isotropic chiral is that the degree of chirality cannot be effectively controlled. To overcome this issue UAC-based structure has been introduced explore the characteristics of SPPs.

The concept of UAC describes chiral materials that possess nondirectional chirality [11]. It is quite easy to manufacture uniaxial chiral medium [12]. The most common method of producing UAC materials is by incorporating small chiral elements within an anisotropic medium [13]. The vapor deposition technique allows for the efficient production of such a medium [17]. UAC mediums are expected to exhibit several fascinating optical properties due to their chirality and anisotropy. In this manuscript, numerical analysis of SPPs at UAC-metal-UAC in the visible spectrum are analyzed. Three cases of UAC medium are studied to demonstrate the influence of chirality and core width on effective mode index (EMI) as the function of wave frequency.

2. Methodology

The schematic view of the planar interface for UAC-metal-UAC is shown in Fig. 1. UAC materials differ from conventional dielectrics by coupling electric and magnetic fields. The constitutive relations express this coupling in terms of chirality. The constitutive relations may take different forms depending on the choice of field vectors used in the relation.

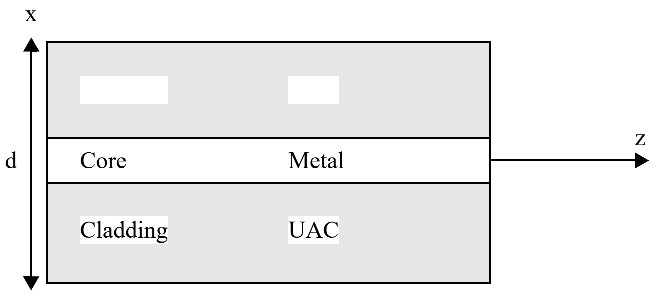

Fig. 1. Schematic view of the planar interface for UAC-metal-UAC.

The brief description of the constitutive relations for uniaxial chiral medium are given below.

$$\mathbf{D} = \left[\varepsilon_t \bar{\bar{I}}_t + \varepsilon_z \hat{e}_z \hat{e}_z\right] \cdot \mathbf{E} - j\xi\sqrt{\mu_0 \varepsilon_0}\, \hat{e}_z \hat{e}_z \cdot \mathbf{H} \tag{1a}$$

$$\mathbf{B} = \left[\mu_t \bar{\bar{I}}_t + \mu_z \hat{e}_z \hat{e}_z\right] \cdot \mathbf{H} - j\xi\sqrt{\mu_0 \varepsilon_0}\, \hat{e}_z \hat{e}_z \cdot \mathbf{E} \tag{1b}$$

In above equation, ξ denote the chirality which is responsible for electromagnetic coupling, $\bar{\bar{I}}_t = \hat{e}_x \hat{e}_x + \hat{e}_z \hat{e}_z$ denote the dyadic vector, ε_0 and μ_0 represent the permittivity and permeability of free space, respectively, ε_t, μ_t, and ε_z, μ_z are transverse and longitudinal components of uniaxial chiral medium, and $\hat{e}_x$, $\hat{e}_y$, and $\hat{e}_z$ are mutually perpendicular unit vectors in a Cartesian coordinate system.

$$E_{z1} = S_1 \exp(-k_p x) + S_2 \exp(-k_n x) \tag{2}$$

$$H_{z1} = \frac{j\alpha_{1,2}}{\eta_t}\left[S_1 \exp(-k_p x) + S_2 \exp(-k_n x)\right] \tag{3}$$

$$E_{z3} = S_3 \exp(k_p x) + S_4 \exp(k_n x) \tag{4}$$

$$H_{z3} = \frac{j\alpha_{1,2}}{\eta_t}\left[S_3 \exp(k_p x) + S_4 \exp(k_n x)\right] \tag{5}$$

As for the remaining EM field components, they obtained as follows: k_p and k_n describe the wavenumbers for UAC medium [18]. The remaining EM fields components can be obtained from [18].

$$k_p^2 = \frac{\lambda^2}{2}\left[\frac{\mu_z}{\mu_t} + \frac{\varepsilon_z}{\varepsilon_t} + \sqrt{\left(\frac{\mu_z}{\mu_t} - \frac{\varepsilon_z}{\varepsilon_t}\right)^2 + \frac{4\xi^2 \mu_z \varepsilon_z}{\mu_t \varepsilon_t}}\right] \tag{6}$$

$$k_n^2 = \frac{\lambda^2}{2}\left[\frac{\mu_z}{\mu_t} + \frac{\varepsilon_z}{\varepsilon_t} - \sqrt{\left(\frac{\mu_z}{\mu_t} - \frac{\varepsilon_z}{\varepsilon_t}\right)^2 + \frac{4\xi^2\mu_z\varepsilon_z}{\mu_t\varepsilon_t}}\right] \tag{7}$$

$$\lambda^2 = \beta^2 - \omega^2\mu_t\varepsilon_t \tag{8}$$

$$\alpha_1 = \left(\frac{k_p^2}{\lambda^2} - \frac{\varepsilon_z}{\varepsilon_t}\right)\frac{\sqrt{\mu_t\varepsilon_t}}{\xi\sqrt{\mu_z\varepsilon_z}} \tag{9}$$

$$\alpha_2 = \left(\frac{k_n^2}{\lambda^2} - \frac{\varepsilon_z}{\varepsilon_t}\right)\frac{\sqrt{\mu_t\varepsilon_t}}{\xi\sqrt{\mu_z\varepsilon_z}} \tag{10}$$

$$\eta_t = \sqrt{\varepsilon_t/\mu_t} \tag{11}$$

$$H_{z2} = S_5\exp(k_m x) + S_6\exp(-k_m x) \tag{12}$$

$$E_{z2} = S_7\exp(k_m x) + S_8\exp(-k_m x) \tag{13}$$

$$E_{y2} = \frac{1}{j\omega\varepsilon_m}\frac{d}{dx}H_{z2} \tag{14}$$

$$H_{y2} = -\frac{1}{j\omega\mu_0}\frac{d}{dx}E_{z2} \tag{15}$$

Here, S_1, S_2, S_3, S_4, S_5, S_6, S_7 and S_8 are unknown coefficient, and

$$k_m = \sqrt{\beta^2 - \omega^2\varepsilon_m\mu_0} \tag{16}$$

$$k_0 = \omega\sqrt{\mu_0\varepsilon_0} \tag{17}$$

while ε_m is the permittivity of metal as reported in [19].

$$\hat{x} \times \left[H_1 - H_2\right] = 0 \tag{18}$$

$$\hat{x} \times \left[E_1 - E_2\right] = 0 \tag{19}$$

The above set of EM fields equations for UAC medium and metal medium, with the boundary conditions for UAC-metal at $x = d$ and for metal-UAC at $x = -d$ interfaces yields the following dispersion relation:

$$-(\alpha_1-\alpha_2)\eta\Big[k_p k_n k_m^2+k_t^2\alpha_1\alpha_2\varepsilon_m\mu_0\omega^2+(k_p k_n k_m^2-k_t^2\alpha_1\alpha_2\varepsilon_m\mu_0\omega^2)\cosh(2dk_m)\Big]$$
$$-k_t(k_n\alpha_1-k_p\alpha_2)k_m(-\varepsilon_m\eta^2+\alpha_1\alpha_2\mu_0)\omega\sinh(2dk_m) = 0 \tag{20}$$

3. Results

In this section, the numerical results for UAC-metal-UAC planar structure are analyzed to calculate the EMI under the different values of chirality and core width d by using dispersion relation (20). The UAC media provide an extra degree of freedom to control the SPPs, in comparison with the isotropic chiral media. It is important to consider the EMI during the fabrication of nano-plasmonic devices in optics sector [20]. In all proposed cases gold metal is assumed.

3.1. Case I

In this case, we have chosen the parameter values as: $\mu_t=\mu_z=\mu_0, \mu_1=1, \varepsilon_t=-0.025\,\varepsilon_0$, $\varepsilon_z=0.2\,\varepsilon_0$ and $\xi=0.7$. To properly investigate the EMI for the UAC-metal-UAC planar structure, the influence of chirality and core width on the EMI are examined in Figs. 2(a) and (b), respectively. According to Fig. 2(a), as chirality increases, the incident wave frequency decreases and EMI increases as reported in [21-23].

Furthermore, the frequency band becomes wider for higher chirality values. It is important to note that at higher frequencies characteristic curves display unphysical regions. Higher ξ values result in larger EMI, indicating that a greater ξ enhances the localization of surface plasmons and their interaction with the material. This can lead to more efficient plasmon propagation at the interface. This is very crucial factor in

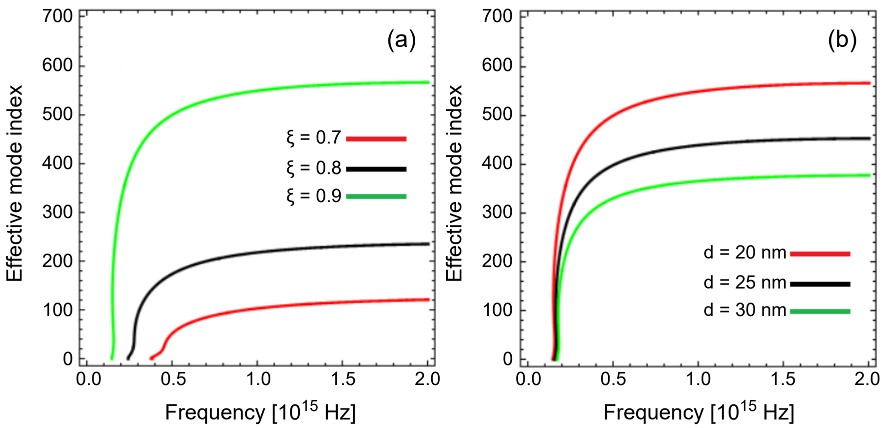

Fig. 2. Influence of chirality on core width on EMI for case I at $\mu_t=\mu_z=\mu_0$, $\mu_1=1$, $\varepsilon_t=-0.025\,\varepsilon_0$, and $\varepsilon_z=0.2\,\varepsilon_0$.

the design of plasmonic sensors, waveguides, and nanoscale optical devices. Thus, increasing chirality results in an increased EMI for SPPs which reflect the stronger field confinement. This is primarily due to the modification of optical properties and coupling mechanisms at the UAC-metal-UAC interface caused by chirality. In plasmonics, the thickness of the metal layer drastically affects the propagation and confinement of surface plasmons. The EMI under the different values of core width is analyzed in Fig. 2(b). As magnitude of core width increases, the EMI decreases [6,24] in the proposed frequency range. Furthermore, frequency band starts squeezing for higher core width values. The change in core width will result in a change in the phase velocity dispersion and group velocity dispersion of the SPPs as well as the field confinement that is extremely suitable for sensors applications as reported in [25]. As seen in Fig. 2(b), thinner layers lead to stronger confinement (higher EMI). This is because in plasmonics, thinner metal layers allow for tighter coupling between the electromagnetic field and the electron oscillations at the surface. Form Fig. 2, it is concluded that by increasing the chirality or reducing the core width, field confinement can be improved, providing benefits for applications such as enhanced spectroscopy and miniature optical circuits.

3.2. Case II

In this case, we have used the parameter values as: $\mu_t = \mu_z = \mu_0$, $\mu_1 = 1$, $\varepsilon_t = 0.25\varepsilon_0$, $\varepsilon_z = -0.2\varepsilon_0$, $\xi = 0.7$ and core width $d = 20$ nm. EMI *versus* incident wave frequency under the different values of chirality is plotted in Fig. 3(a). In UAC, medium when EM waves interact with chiral molecules, the behavior of SPPs is changed. With increasing chirality, characteristics peaks are shifted from low to high frequencies. Furthermore, by increasing the chirality parameter, the frequency band becomes wider. This broadening of the frequency band is caused by chiral interactions between the electromagnetic wave and metal medium, which modify the behavior and response of the

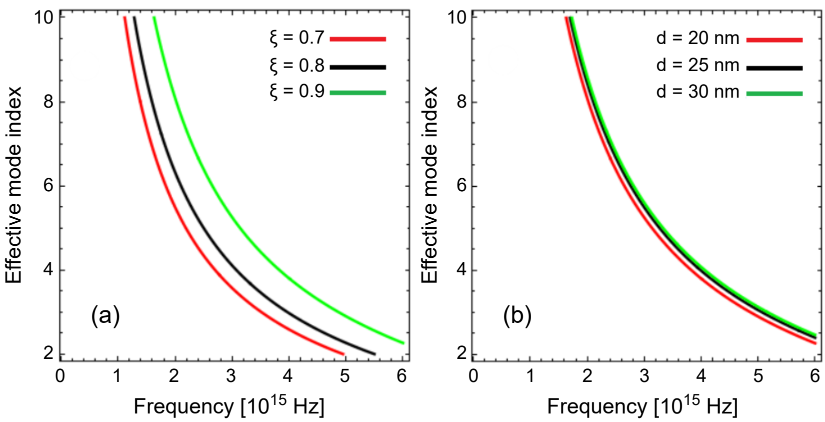

Fig. 3. Impact of chirality and core width on EMI for case II at $\mu_t = \mu_z = \mu_0$, $\mu_1 = 1$, $\varepsilon_t = 0.25\varepsilon_0$, and $\varepsilon_z = -0.2\varepsilon_0$.

SPPs for proposed waveguide structure. Furthermore, the cut-off frequency starts to increase by increasing chirality value. Moreover, the highest EMI is achieved for highest value of chirality as reported in [21-23]. Figure 3(b) illustrates the effect of core width on EMI *versus* incident wave frequency. In response to the increase in core width, the SPPs mode interacts more strongly with the surrounding UAC medium. Additionally, larger core width values reduce the amount of SPPs mode leakage into the UAC medium. Like case I, the frequency band starts squeezing with the increment of core width. Furthermore, as core width increases, the EMI increases as reported in [19] for case II. The results indicate that higher values of core width could result in higher EMI in the proposed frequency range. Moreover, the highest variation in characteristics peak occurs for lower core width as indicated by red peak. Compared to case I, it is seen that core widths have a very small influence on EMI for case II. Overall, these attributes are crucial for high frequency plasmonic devices where tuning chirality and core width can achieve desired field distribution and mode stability.

3.3. Case III

In this case, we have used the parameter values as: $\mu_t = \mu_z = \mu_0$, $\mu_1 = 1$, $\varepsilon_t = -0.25\varepsilon_0$, $\varepsilon_z = -0.5\varepsilon_0$, $\xi = 0.7$ and core width $d = 20$ nm. In Fig. 4(a) we plot the EMI under the different values of chirality by using characteristics Eq. (20). The cut-off frequency decreases as chirality increases while EMI increases, indicating a stronger confinement of SPPs. As compared to the previous cases, *i.e.*, case I and case II, it is particularly noteworthy that case III supports very high frequencies and displays the lowest EMI. The numerical results suggest that if both ε_t and ε_z have negative values then SPPs will be generated at very high frequencies with the lowest effect mode index when compared to other cases discussed above for the proposed waveguide structure. In waveguides, the dispersion relation of SPPs modes is strongly affected by the geometry of the waveguide, including the width of its core. So, the dispersion properties of an SPPs mode

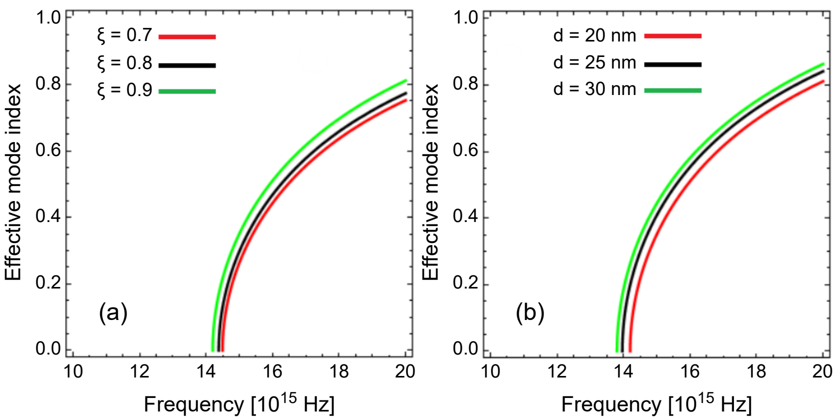

Fig. 4. Impact of chirality and core width on EMI for case II at $\mu_t = \mu_z = \mu_0$, $\mu_1 = 1$, $\varepsilon_t = -0.25\varepsilon_0$, and $\varepsilon_z = -0.5\varepsilon_0$.

can be modified by varying core width of waveguide. To study the factor of EMI, which is a very important parameter for the plasmonic sector, Fig. 4(b) analyzes the influence of core width on EMI. The core width increases from $d = 20$ nm to $d = 30$ nm. Like the previous two cases, as core width increases, the frequency band becomes broadened. Furthermore, the highest EMI could be achieved at the highest value of core width in the proposed frequency band for proposed waveguide structure. This is because increasing the core width allows for more effective confinement of the electromagnetic field within the waveguide. As a result, the interaction between the core and cladding is enhanced, leading to an increase in the effective mode index (EMI). This makes the waveguide more efficient at guiding light at high frequencies. As core width increases, leakage losses decrease and mode confinement increases near the UAC-met-

Table 1. Frequency and effective mode index for case I.

Frequency [10^{15} Hz]	Effective mode index	Frequency [10^{15} Hz]	Effective mode index
2	121.0636	0.520833	57.7747
1.665214	117.9813	0.506297	53.77604
1.390625	113.8076	0.494792	49.98038
1.213542	109.9861	0.484375	45.92148
1.073613	105.973	0.475783	41.92708
0.968998	101.9965	0.46875	37.93317
0.885417	97.97503	0.462952	33.9304
0.817708	93.93696	0.457686	29.6224
0.760417	89.99538	0.453125	25.54552
0.712665	85.98389	0.448477	21.67885
0.667918	81.59345	0.440713	17.10467
0.63653	77.99576	13.74401	13.74401
0.606317	73.98685	0.416667	9.54575
0.580065	69.94977	0.398438	5.954142
0.557292	65.87333	0.376376	1.822917
0.537915	61.97917	0.3845	0

Table 2. Frequency and effective mode index for case II.

Frequency [10^{15} Hz]	Effective mode index
1.112843	10
1.233528	9
1.383478	8
1.57467	7
1.826032	6
2.170534	5
2.668641	4
3.442455	3
4.7539	2

T a b l e 3. Frequency and effective mode index for case III.

Frequency [10^{15} Hz]	Effective mode index
20	0.752623
19.02028	0.702138
18.00092	0.637408
17.07451	0.5625
16.00019	0.443769
15	0.264003
14.49511	0

al-UAC planar interface, ultimately leading to an increase in the EMI. Thus, from Fig. 4, a fine control of chirality and d is crucial in the development of narrowband plasmonic devices. Case I can greatly improve field localization and sensitivity in applications such as waveguides, modulators, and sensors used in THz plasmonics. Case II can be advantageous for compact and efficient THz devices, such as resonators and sensors, where field confinement is essential. While case III is crucial in the development of narrowband plasmonic devices.

The data table regarding effective mode index and frequency for cases I–III are given in Tables 1–3, respectively.

4. Conclusion

The numerical analysis of SPPs at UAC-metal-UAC planar waveguide structure has been analyzed. Three cases of UAC media were analyzed in the visible frequency range. It has been demonstrated that highest EMI achieved when $\varepsilon_t < \varepsilon_z$ and lowest EMI achieved when both ε_t and ε_z are negative. When $\varepsilon_t < \varepsilon_z$, lower frequency plasmon mode is generated but when both ε_t and ε_z are negative, higher frequency plasmon mode are generated. Furthermore, it is also concluded that higher values of core width reduce the EMI for case I and *vice versa* for cases II and III. This study can be advantageous for compact and efficient THz devices, such as resonators, modulators and sensors where field confinement is essential.

Acknowledgments

The authors would like to thank King Saud University, Riyadh, Saudi Arabia for Supporting through Ongoing Research Funding Program (ORF-2025-416).

Funding

This work was supported by the Researchers Supporting Project number (ORF-2025-416). King Saud University, Riyadh, Saudi Arabia.

Declaration of competing interest

The authors declare that they have no known competing financial interests or personal relationships that could have appeared to influence the work reported in this paper.

Authors' contributions

M. Umair wrote main manuscript and derived analytical expressions. A. Ghaffar and Majeed A.S. Alkanhal edited the manuscript and reviewed the numerical analysis. Y. Khan and M. Amir Ali developed methodology in the given study. All authors reviewed the manuscript before submission.

References

[1] Gric T., *Surface-plasmon-polaritons at the interface of nanostructured metamaterials*, Progress In Electromagnetics Research M **46**, 2016: 165-172. https://doi.org/10.2528/PIERM15121605

[2] Gric T., Hess O., *Tunable surface waves at the interface separating different graphene-dielectric composite hyperbolic metamaterials*, Optics Express **25**(10), 2017: 11466-11476. https://doi.org/10.1364/OE.25.011466

[3] Sana T., Alkanhal M.A.S., Ali A., Ullah H., Ghaffar A., Khan Y., Yaqoob M.Z., *Thermally tunable phonon–plasmon polariton modes at hexagonal boron nitride (hBN) and indium antimonide (InSb) interfaces*, Journal of Optics **26**(11), 2024: 115006. https://doi.org/10.1088/2040-8986/ad8459

[4] Yaqoob M.Z., Ghaffar A., Alkanhal M.A.S., Aladadi Y.T., *Analysis of hybrid surface wave propagation supported by chiral metamaterial–graphene–metamaterial structures*, Results in Physics **14**, 2019: 102378. https://doi.org/10.1016/j.rinp.2019.102378

[5] Bousbih R., Soliman M.S., Jafar N.N.A., Jabir M.S., Majdi H., Alshomrany A.S., Hadia N.M.A., Shaban M., El-Badry Y.A., Iftikhar M., *Generation of surface plasmon polaritons (SPPs) at chiro-plasma-metal interface*, Plasmonics **20**, 2025: 863-868. https://doi.org/10.1007/s11468-024-02328-y

[6] Kwon M.-S., *Metal-insulator-silicon-insulator-metal waveguides compatible with standard CMOS technology*, Optics Express **19**(9), 2011: 8379-8393. https://doi.org/10.1364/OE.19.008379

[7] Mi G., Van V., *Characteristics of surface plasmon polaritons at a chiral–metal interface*, Optics Letters **39**(7), 2014: 2028-2031. https://doi.org/10.1364/OL.39.002028

[8] Saeed M., Ghaffar A., Alkanhal M.A.S., Khan Y., *Characteristics of hybrid surface plasmon polaritons at a chiral graphene metal interface in cylindrical waveguides*, Optical and Quantum Electronics **53**, 2021: 560. https://doi.org/10.1007/s11082-021-03219-w

[9] Zhang Q., Li J., Liu X., Gelmecha D.J., *Dispersion, propagation, and transverse spin of surface plasmon polaritons in a metal-chiral-metal waveguide*, Applied Physics Letters **110**(16), 2017: 161114. https://doi.org/10.1063/1.4982158

[10] Zheng Y., Chen J., Ji Z., Lin H., Li Z.-Y., *Analytical solutions for electromagnetic surface states at the interface between metal and gyromagnetic media*, Journal of the Optical Society of America B **40**(11), 2023: 2815-2828. https://doi.org/10.1364/JOSAB.499881

[11] Palik E.D., *Handbook of Optical Constants of Solids*, Vol. 3., Academic Press, 1998.

[12] Novotny L., Hecht B., *Principles of Nano-Optics*, Cambridge University Press, 2012.

[13] Zhang Q., Li J., *Characteristics of surface plasmon polaritons in a dielectrically chiral-metal -chiral waveguiding structure*, Optics Letters **41**(14), 2016: 3241-3244. https://doi.org/10.1364/OL.41.003241

[14] Baqir M.A., Choudhury P.K., *Propagation through uniaxial anisotropic chiral waveguide under DB-boundary conditions*, Journal of Electromagnetic Waves and Applications **27**(6), 2013: 783-793. https://doi.org/10.1080/09205071.2013.786209

[15] Dong J.-F., Li J., *Guided modes in the circular waveguide filled with uniaxial chiral medium*, International Journal of Applied Electromagnetics and Mechanics **40**(4), 2012: 283-292. https://doi.org/10.3233/JAE-2012-1591

[16] Ghaffar A., Alkanhal M.A.S., *Electromagnetic reflection and transmission from a planar isotropic chiral-uniaxial chiral interface with optical axis normal to interface*, International Journal of Applied Electromagnetics and Mechanics **47**(3), 2015: 805-817. https://doi.org/10.3233/JAE-130161

[17] Naheed M., Faryad M., *Excitation of surface plasmon–polariton waves in the prism-coupled configurations guided by reciprocal, uniaxially chiral, bianisotropic material*, Optics Communications **465**, 2020: 125611. https://doi.org/10.1016/j.optcom.2020.125611

[18] Ghaffar A., Alkanhal M.A.S., *Electromagnetic waves in parallel plate uniaxial anisotropic chiral waveguides*, Optical Materials Express **4**(9), 2014: 1756-1761. https://doi.org/10.1364/OME.4.001756

[19] Umair M., Ghaffar A., Alkanhal M.A.S., Khan Y., Alqahtani A.H., Shakir I., *Plasmonic modes of metallic slab in anisotropic plasma environment*, Plasmonics **18**, 2023: 1857-1864. https://doi.org/10.1007/s11468-023-01903-z

[20] Umair M., Ghaffar A., Alkanhal Majeed A.S., Khan Y., Shahid M.U., *Dyakonov waves generation at uniaxial chiral-plasma interface*, Optics Express **32**(3), 2024: 4376-4386. https://doi.org/10.1364/OE.510362

[21] Umair M., Ghaffar A., Razzaz F., Saeed S.M., *Hybrid plasmon modes at chiroferrite-graphene interface*, Plasmonics **19**, 2024: 2193-2199. https://doi.org/10.1007/s11468-023-02148-6

[22] Xu J.-P., *Propagation characteristics of a circular waveguide filled with a chiroferrite medium*, International Journal of Infrared and Millimeter Waves **17**, 1996: 193-203. https://doi.org/10.1007/BF02088193

[23] Umair M., Ghaffar A., Alkanhal M.A.S., Khan Y., Alqahtani A.H., *Light plasmon coupling in planar chiroplasma–graphene waveguides*, Plasmonics **18**, 2023: 1029-1035. https://doi.org/10.1007/s11468-023-01824-x

[24] Umair M., Ghaffar A., Alkanhal M.A.S., Alqahtani A.H., Khan Y., *Transverse electric surface waves in ferrite medium surrounded by plasma layers*, Journal of the European Optical Society - Rapid Publications **16**, 2020: 17. https://doi.org/10.1186/s41476-020-00138-3

[25] Zhang X., Xu Q., Xia L., Li Y., Gu J., Tian Z., Ouyang C., Han J., Zhang W., *Terahertz surface plasmonic waves: A review*, Advanced Photonics **2**(1), 2020: 014001. https://doi.org/10.1117/1.AP.2.1.014001

Received November 8, 2024
in revised form December 30, 2024